

ANALYSIS OF EFFICIENCY ENHANCEMENT OF FLAT PLATE SOLAR COLLECTOR USING NANOFLUIDS

K. Farhana^{1,4}, K. Kadirgama¹, R. Saidur^{2,5}, D. Ramasamy¹, A. S. F. Mahamude³

¹Faculty of Mechanical Engineering, Universiti Malaysia Pahang, 26600 Pekan, Pahang, Malaysia

²Research Centre for Nano-Materials and Energy Technology (RCNMET), Sunway University, Bandar Sunway, Malaysia

³Faculty of Chemical & Natural Resources Engineering, Universiti Malaysia Pahang, 26300 Gambang, Pahang, Malaysia

⁴Department of Apparel Manufacturing Engineering, Bangladesh University of Textiles, Dhaka 1208, Bangladesh

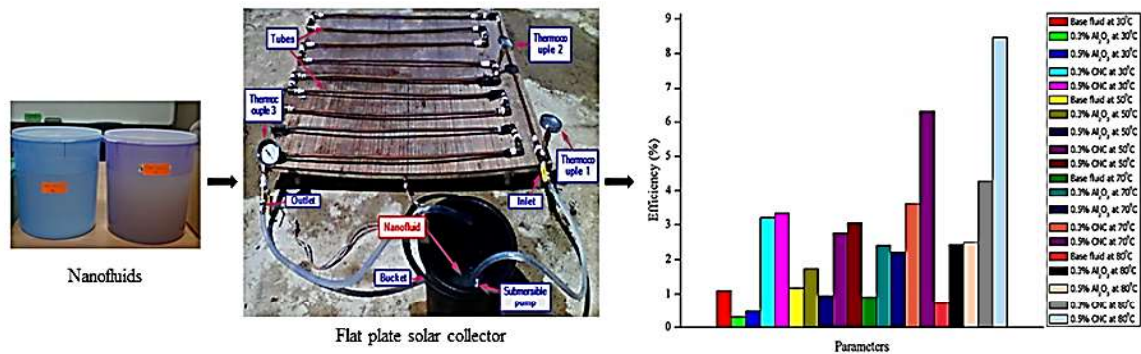
⁵Department of Engineering, Lancaster University, LA1 4YW, United Kingdom

Corresponding author: kfarnaha81@yahoo.com, kumaran@ump.edu.my

Abstract

This study analyses the efficiency enhancement of flat plate solar collector using Al₂O₃ and crystal nano-cellulose (CNC) nanofluids. The upward energy demand along with the depletion of conventional energy sources demands improved utilization of renewable energy resources. Among all renewable energy resources, solar energy is the most appropriate alternative to conventional energy sources owing to its inexhaustibility and green property. Solar collectors are devices that convert solar radiation into heat or energy. However, the efficiency of the solar collector is still not adequate. The competent step to enhance the efficiency of the solar collector is to use nanofluids. This study is carried out different phases viz. characterization and stabilization while both qualitative and quantitative methods used to evaluate the stability of nanofluids; several thermo-physical properties of Al₂O₃ and CNC nanofluids such as thermal conductivity measured at four different temperature using KD2 Pro, viscosity and specific heat determined at similar temperature range by viscometer and differential scanning calorimetry respectively; implementation of nanofluids in the solar collector. The experiment is executed with a fixed flow rate and in steady-state conditions under open solar radiation. The experimental study has revealed that up to 2.48% and 8.46% efficiency of solar collector enhanced by using 0.5% Al₂O₃ and 0.5% CNC nanofluids respectively. Moreover, nanofluids show good to moderate stability performance. In addition, the thermal conductivity of nanofluids increased while viscosity is in decreasing trend with increasing temperature. Applying nanofluids could enhance the efficiency of a flat-plate solar collector.

Graphical abstract



Keywords: Nanofluids; Thermo-physical Properties; Flat Plate Solar Collector; Energy Gain; Efficiency

1. Introduction

To fulfill the smart demands of people, the utilization of energy is increasing day by day. As a result, the depletion of fossil energy, as well as its unfavorable response, urges to realize to take necessary actions rapidly [1, 2]. Therefore, renewable energies are trying to capture the space of fossil energy. solar energy is the most preferable energy among various renewable energies as it is inexhaustible, clear and plentiful [3, 4]. To harvest solar energy, the solar collector is one of the most important devices and green invention as well [5]. Solar collector suffering from low energy efficiency. But efficiency can be improved by replacing the working fluids into nanofluids [6]. Newly developed solar collector which is simple and has a wide range of applications specifically in domestic and industrial usages to heat water named flat plate solar collector (FPSC). Although FPSC has a versatile implementation, it is suffering from low energy efficiency. Nanofluid is the most promising and latest method to enhance the efficiency of FPSC [7, 8].

Nomenclature

ASHRAE	The American Society of Heating, Refrigerating and Air Conditioning Engineers
Al ₂ O ₃	Aluminium Oxide
CNC	Crystal nano-cellulose
CSR	Controlled shear rate
CuO	Copper Oxide
DSC	Differential scanning calorimetry

DWCNT	Double-Walled Carbon Nanotube
EDX	Energy dispersive x-ray spectroscopy
EG	Ethylene glycol
ELS	Electrophoretic light scattering
FESEM	Field emission scanning electron microscopy
FLIR	Forward-looking infrared
FPSC	Flat plate solar collector
MWCNT	Multi-Walled Carbon Nanotube
MgO	Magnesium Oxide
SiO ₂	Silicon Dioxide
SWCNT	Single-Walled Carbon Nanotube
TEM	Transmission electron microscopy
TiO ₂	Titanium Dioxide
W	Water
ZnO	Zinc Oxide
ZrO ₂	Zirconium Dioxide
<i>Greek symbols</i>	
ϕ	Volumetric concentration of particles (%)
C_p	Specific heat (J/g-K)
w	Mass fraction
Q_u	Energy gain (kW)
\dot{m}	Mass flow rate (kg/s)
I_t	Incident solar radiation (W/m ²)
A_c	Area of the solar collector (m ²)
η	Efficiency (%)
T	Temperature (K or °C)
τ	Shear stress
γ	Shear rate
<i>Subscripts</i>	
p	Particle
bf	Base fluid

Nanofluid is the latest approach for modern technology to enhance the performance of engineering tools and machinery [9]. Nanofluids prepared by dispersing the nanoparticles into the base fluids [10, 11]. Nanoparticles enable unique properties such as physicochemical, optical and biological properties which can be manipulated suitably in the intended application [12, 13]. Thermal conductivity and heat transfer coefficient increased significantly by adding a tiny number of nanoparticles into the working fluids as well as further enhancement occurred linearly due to the augmentation of nanoparticles into the base fluid. Moreover, nanofluid exhibits the enhancement of heat transfer, improved suspension stability, high surface volume, fewer particles clogging and anomalous increase in thermal conductivity while the heat transfer or heat transfer coefficient directly related to thermal conductivity. Water and ethylene glycol have been utilized in much nanofluid related research works as a base fluid. However, nanofluids are not only great interest to increase the heat transfer but also improving other properties such as rheological behaviour and mass transfer properties [14-16].

The researchers and scientists have experimented and identified different types of metallic nanoparticles such as Al, Fe, Cu, Ag, and Au; non-metallic nanoparticles such as CuO, SiC, Al₂O₃, ZnO, semiconductors (TiO₂), carbon nanotubes (SWCNT, DWCNT, MWCNT) and composites materials such as nanoparticles core polymer shell composites; while most of them are chemically stable and functionalized nanoparticles. Generally, nanoparticles produced by physical and chemical synthesis techniques [17, 18]. In addition to this, over the last few years nano-cellulose attract more attention to the researchers due to some of their notable properties such as biodegradability, impressive mechanical properties, lower density, plentiful in nature and most importantly eco-friendly aspect as well [19, 20].

In the last few years, the researchers are studying more on the efficiency enhancement of flat plate solar collectors using nanofluids as working fluids in replace of conventional fluids such as Yousefi, Veisy [21] studied the thermal performance of FPSC with MWCNT-water nanofluid and concluded the improvement of collector significantly. Moghadam, Farzane-Gord [22] studied the efficacy of an FPSC increase of 16.7% when CuO-water nanofluid applied in the solar collector. Said, Sabiha [23] experimentally investigated the output temperature enhancement of FPSC using TiO₂-water nanofluid. The authors revealed that nanofluids can maximize the temperature up to 65°C. In addition, Verma, Tiwari [24] studied the efficiency of FPSC using MgO-water nanofluid and revealed that the efficacy of collector enhanced. Later, Verma, Tiwari [25] again investigated the efficiency performance of FPSC by using various nanofluids such as CuO, TiO₂, MWCNT, Graphene/water nanofluids and found that

the MWCNT nanofluid shows the highest increment of efficiency of FPSC. Besides, Ziyadanogullari, Yucel [26] studied the thermal performance of FPSC using Al₂O₃, TiO₂, CuO/water nanofluids. The authors concluded that the maximum efficiency of collector achieved by using CuO-water nanofluid while the lowest increase found for TiO₂-water nanofluid. Eltaweel and Abdel-Rehim [27] experimentally investigated the efficiency performance of FPSC with MWCNT-water nanofluid. They revealed that the efficiency of 16%, 21%, and 34.13% was higher than distilled water at the concentration of 0.01 wt%, 0.05 wt%, and 0.1 wt% nanofluids respectively.

This study aims to analyse the efficiency improvement of the flat plate solar collector by using nanofluids. The focus will be on the inorganic (Al₂O₃) and organic (CNC) nanofluids implementation in FPSC successively, which is incomparable with any study in the literature. Moreover, in this study, the efficiency of FPSC will be analysed considering the tubes (header and riser) of FPSC through which the nanofluids can circulate. Thereby, the Al₂O₃ and CNC nanoparticles will be characterized and prepared by standard method; thermo-physical performances of nanofluids will be evaluated and finally, nanofluids will be applied in FPSC to observe the efficiency enhancement of collector in the steady-state condition under solar radiation. The result will be compared with other studies which are near it.

2. Material and Methods

In this study, aluminium oxide (Al₂O₃) anhydrous nanoparticles used which was procured from Bendosen Laboratory Chemicals. CNC nanoparticle used and was purchased from Blue Goose Biorefiners Inc. company with a weight concentration of 8.0% w/w. The specification of CNC nanoparticles was provided by the company as presented in Table 1. EG with water (W: EG 60: 40 ratio) has been selected as the base or working fluids.

Besides, the specification of flat plate solar collector (FPSC) especially the tubes (header and riser) has been described in Table 2. The efficiency of FPSC has been calculated by the following (Eq. (1 and 2)).

$$Q_u = \dot{m} C_p T_{out} - T_{in} \quad (1)$$

$$\eta = \frac{Q_u}{I_t A_c} \quad (2)$$

Where η is the efficiency (%); Q_u is the energy gain (kW); \dot{m} is the mass flow rate (kg/s); C_p is the specific heat (J/g-K); I_t is the solar radiance (W/m²); A_c is the total area of the solar collector (m²); T_{out} and T_{in} are the outlet and inlet temperature (°C) respectively. Moreover, In this study, solar radiance has been considered as a constant value of 830 W/m² which was selected from the experimental work of solar collector performed by Gaos, Yulianto [28]. The authors found the maximum average value of solar radiance was 830 W/m² during the evaluation of the performance of the solar collector significantly.

2.1 Characterization and Preparation of Nanofluids

The nanoparticles (Al₂O₃ and CNC) were characterized by using different characterization equipment such as Field-emission scanning electron spectroscopy (FESEM), Transmission electron microscopy (TEM) [29-32]. In this study, the two-step method has been used to prepare the nanofluids as similar to many previous studies such as Ramachandran, Hussein [33] and Azmi, Hamid [34]. Nanoparticles (Al₂O₃ and CNC) were suspended in the base fluid (W: EG 60:40) at different volume fractions such as 0.1%, 0.3%, and 0.5% and then mixed/blended it using a magnetic stirrer until proper mixing. The required mass of nanoparticles in a dry form corresponding to the volume concentration was calculated using (Eq.(3)) [35].

$$\phi = \frac{\frac{w}{\rho_p}}{\frac{w}{\rho_p} + \frac{w_{bf}}{\rho_{bf}}} \times 100 \quad (3)$$

Where ϕ is the volume concentration of nanofluids (%), w is the mass fraction and ρ stands for density. The subscripts p and bf stand for nanoparticles and base fluid respectively.

Afterward, sonication has been done using probe sonication processor until no agglomerates could be observed in the suspension [36]. Fig. 1 shows the preparation method for nanofluids. Sonication of nanofluids is very necessary to prepare stable nanofluids by disperse the nanoparticles into the base fluids uniformly and to avoid agglomeration or agitation of nanoparticles.

2.2 Measurement of Thermo-physical Properties

The stability of Al₂O₃ and CNC nanofluids have been measured by qualitative and quantitative methods. In the case of the quantitative method, to measure the stability of both nanofluids

litesizer 500 zeta potential (Anton Paar, Austria) used. ELS (electrophoretic light scattering). Omega Cuvette measurement cell used to evaluate the electro kinetic potential in colloidal dispersion. The zeta potential values obtained in the millivolt [37]. Sedimentation observation (Qualitative method) has been done by naked eyes to examine the stability of Al₂O₃ and CNC nanofluids at various volume concentrations similarly with Kadirgama, Anamalai [38] conducted the qualitative method to measure the stability of nanofluids in thermal analysis of SUS 304 stainless steel using nano-cellulose/ethylene glycol-based study.

Thermal conductivity of the base fluid, Al₂O₃, and CNC nanofluid at 0.1%, 0.3%, and 0.5% volume concentrations were measured by KD2 Pro Thermal Property Analyser (Decagon Devices, Inc., USA). The transient hot-wire method was the operating principle of that device. KD2 Pro consists of a handheld controller and a sensor. This sensor can measure the thermal conductivity between 0.002-2.00 W/m-K with an accuracy of ±5%. The experiment was performed at a temperature range of 30°C to 80°C (controlled condition). Before starting the actual sample measurement, the sensor was validated by measuring the thermal conductivity of glycerine (k= 0.282 W/m-K at 20°C; solution provided by the manufacturer. Moreover, the thermal conductivity measurement verified by measuring the base fluid (60% water and 40% ethylene glycol) and compared with predetermined values of ASHRAE standard (American Society of Heating, Refrigerating and Air Conditioning Engineers). The maximum deviation between the base fluid and ASHRAE data was 3.2%. Previously many researchers used KD2 Pro Thermal Property Analyser to measure the thermal conductivity of nanofluids in experimental studies [39-42].

In this study, the dynamic viscosity of CNC nanofluids with various volume concentrations was measured at a temperature range of 30°C to 80°C by Brookfield RST, Coaxial Cylinder rheometer. And the dynamic viscosity of Al₂O₃ nanofluids measured at the same range of temperature by Malvern Panalytical (model Kinexus lab+) manufactured by Malvern Panalytical Ltd, United Kingdom. At first, the viscosity of base fluid was measured and compared the obtained values with the prementioned data of the ASHRAE standard. The rotational measurement under controlled shear rate (CSR) method used. Previously many studies used Brookfield RST and Malvern Panalytical in order to measure the viscosity of nanofluids [34, 43].

Differential scanning calorimetry (DSC) is a highly sensitive technique can be used to measure the specific heat capacity (C_p) of both solid and fluids [44, 45]. Here specific heat of nanofluids

(both Al_2O_3 and CNC) at various volume concentrations has been measured using the Linseis DSC 1000 (Differential scanning calorimetry-Germany). In this study, the weight of all samples was fixed at 13 mg weighing by electrical balance and that has been loaded in aluminium crucibles. Fig. 2 shows the specific heat measurement tools. This equipment gives the highest possible accuracy of C_p by using modulated heating rate temperature profiles. This method defines a steady change in the heat flow of the samples and the system can observe the heat uptake superiorly than a linear heating system [46]. Besides, C_p measurement could be affected by the mass value of the materials and the heating rate owing to the use of the DSC [47].

2.3 Application of Nanofluids in FPSC

Two types of volume concentrations have been preferred based on the performance of thermo-physical properties of both (Al_2O_3 and CNC) nanofluids such as 0.3% and 0.5% to apply in FPSC. The experiment has been run during day time (sunny day) from 10.00 am to 2.00 pm and the location was University Malaysia Pahang [48]. Forward-looking infrared (FLIR) thermal camera has been used to measure the surface temperature of copper tubes. Fig. 3 presents the experimental setup and Table 3 shows the list of apparatus of the experimental setup of the collector with properties.

Prior to starting the measurement of temperature by FLIR thermal camera, FLIR has been calibrated by sensing the temperature of hot water. To avoid the error data ten reading has been taken in maximum temperatures and calculated the average of the hot water around 84.94°C . Before applying the nanofluids in FPSC, the flow rate of the submersible pump has been checked with water by adjusting the flow control of the pump. At the very beginning of the running of this experiment, the inner and outer thermocouple shows the unprecedented temperature difference data between them. To ignore this error reading, three types of observation has been done. After starting equipment, the data has been checked after 10 min, 30 min, and 60 min consecutively; the stable temperature difference was observed between the inlet and outlet of the equipment. Fig. 4 presenting the whole process flow of practical work. However, the temperature difference between inlet and outlet has been evaluated at the lowest and highest flow rate of the pump. The flow rate does not have any significant effect on it.

Around 2000 ml nanofluid has been prepared for each type of nanoparticles (Al_2O_3 and CNC). The volume concentrations were 0.3% and 0.5%. These four-volume concentrations of

nanofluids have been loaded in bucket one after another and the lowest flow rate has been set in the pump. This method has been done in a steady-state condition under direct solar radiation.

3. Result and Discussion

3.1 Characterization of Nanofluids

The size of Al_2O_3 nanoparticles was below 80 nm and most of the particles were spherically determined by using FESEM, as shown in Fig. 5. The elemental composition of nanoparticles was analysed by means of FESEM EDX with 10 μm , 20 μm , and 60 μm electron image. The EDX spectrum shows the presence of aluminium (Al) and oxygen (O) atoms (Fig. 6) and Table 4 depicts the EDX results of the elemental proportion of Al_2O_3 nanoparticle with 20 μm electron image [49].

In addition, the shape and size of solid nanoparticles into the base fluid that is in nanofluid form can also be measured by TEM image [50] as shown in Fig. 7. Moreover, the dispersion of nanoparticles into the base fluid should be defined precisely. Fig. 7 illustrates that most of the nanoparticles of Al_2O_3 nanofluids were nearly spherical and nearly elongated geometry in morphological shape. Nanoparticles were also better uniform in shape and size. The nanoparticles were dispersed evenly into base fluids but often agglomerated into small aggregation.

Apparently, CNC nanoparticles were in gel form and it was not possible to evaluate it morphologically using FESEM. Therefore, CNC nanoparticles have been prepared into two forms such as film and powder to analysis it in FESEM. Fig. 8 shows the morphology of CNC nanoparticles in film form in Fig. 8(a)) and in powder form in Fig. 8(b). The size and shape of nanoparticles could not be measured using FESEM as there were no individual nanosized particles observed in the figure though the samples were dried. Fig. 8 showed the CNC nanoparticles clung with each other. However, the elemental analysis has been done using FESEM EDX. EDX did with 10 μm , 20 μm and 60 μm electron image similar to Al_2O_3 nanoparticles.

The EDX spectrum showed that the clear appearance of carbon (C) and oxygen (O) atoms in CNC nanoparticles as shown in Fig. 9. Besides, Table 5 illustrates the chemical composition of 20 μm electron image of CNC nanoparticles with standard deviation [51]. The TEM micrograph of CNC nanoparticles (powder form) and CNC nanofluids showed in Fig. 10 and Fig. 11 respectively. The size and shape of the CNC nanoparticles determined by Fig. 10. In

this micrographic view, it was observed that the size of the CNC nanoparticles was less than 50 nm. The shape of nanoparticles was in both elongated and nearly spherical geometry. On the other hand, Fig. 11 represents the dispersion phenomenon of CNC nanofluids into the base fluid. The dispersion was not enough fairly even as some aggregation of nanoparticles was obtained due to strong Van der Waals force between the nanoparticles [52].

3.2 Analysis of Thermo-physical Properties

3.2.1 Stability Analysis

Both qualitative and quantitation method has been applied to evaluate the stability of Al_2O_3 and CNC nanofluids. In case of sedimentation observation (Qualitative method), the stability of Al_2O_3 and CNC nanofluids have been examined at various volume concentrations which is similar with Ramachandran, Kadirgama [53] experimental study on effective thermal conductivity and relative viscosity of CNC/water-EG nanofluids through a combined experimental and statistical approach. The authors evaluated the stability of nanofluids by sedimentation observation. In this study, the observation has been done every day. No aggregation of Al_2O_3 and CNC nanoparticles observed at the bottom of the test tube after one week of nanofluids preparation as shown in Table 6. This observation demonstrates the moderate to good stability of both nanofluids meanwhile the numerical values of stability have been investigated by quantitative methods.

From the quantitative method point of view, measurement of the zeta potential of nanofluids is one of the techniques used to evaluate the stability of nanofluids by analyzing electrophoretic behaviour [54]. The measured value of zeta potential above 30 mV is considered to be a good stable nanofluid [11]. The absolute zeta potential values of all nanofluids are presented in Fig. 12. The highest zeta potential value is about 36.1 mV of 0.3% Al_2O_3 nanofluids followed by 0.5% Al_2O_3 nanofluid with 33.6 mV. While 0.1% and other three-volume concentrations of CNC nanofluids showed the absolute value of zeta potential is less than 30 mV. Meanwhile, the Al_2O_3 nanofluids showed positive charge and CNC exhibited negativity potential behaviour. Long term physical and chemical stability of nanofluids is one of the fundamental requirements for its proper usage in heat transfer applications [54]. Because strong Van der Waals interactions of nanoparticles create clusters/aggregation causing non-homogeneity of nanofluids. Moreover, sedimentation of nanoparticles degrades the thermo-physical properties such as thermal conductivity, density, viscosity, specific heat capacity as stability of nanofluids has a significant effect on thermal conductivity directly or indirectly [55]. Aggregation of

nanoparticles within the nanofluids can block the tubes which are responsible for discontinuation of heat transfer and resulting deflation of advantages of nanofluids in heat transfer [56].

3.2.2 Thermal Conductivity Analysis

The thermal conductivity of the base fluid (60% water and 40% EG), Al_2O_3 and CNC nanofluids with different volume concentrations (0.1%, 0.3%, and 0.5%) measured at four different temperatures such as 30°C, 50°C, 70°C, and 80°C. Thermal conductivity of working fluids increased anomalously due to adding nanoparticles into base fluids and Fig. 13 shows the enhancement of thermal conductivity of nanofluids (Al_2O_3 and CNC) at 0.1%, 0.3%, and 0.5% volume concentrations. Despite the increment phenomena of thermal conductivity; 0.1% CNC, nanofluid exhibited a slight decrement of thermal conductivity at a temperature of 50°C and 70°C. However, Al_2O_3 exhibited the increment of thermal conductivity consistently. Moreover, the thermal conductivity increases with an increase in temperature as well [33, 34]. Fig. 13 illustrates that the enhancement of thermal conductivity is not linear with linearly increased volume concentration percentage of nanoparticles at any temperature. This similar phenomenon also observed by Wei, Zou [57]. The authors found thermal conductivity enhancement is not even with increased in volume concentration at a temperature of 20°C. Prior to the experiment with nanofluids, the thermal conductivity of the base fluid (W: EG 60:40) measured to evaluate the measurement accuracy of KD2 Pro Thermal Property Analyser. The error percentage between resulting data and ASHRAE standard of base fluid has been analysed and shown in Fig. 14 which defines the good agreement with the measurement accuracy of the thermal conductivity equipment as well as the thermal conductivity characteristic of the experimental base fluid. The reason for thermal conductivity enhancement can be discussed by the experimental study of Wen and Ding [58]. The authors studied that the nanoparticles in the base fluid increase the thermal conductivity by reducing thermal boundary layer thickness causing convection heat transfer enhancement. Not only that, the migration of nanoparticles in the based fluid is one of the roots of heat transfer enhancement which forms non-uniform distribution of thermal conductivity and viscosity field due to Brownian motion, shear action and spatial gradient in viscosity [59].

3.2.3 Dynamic Viscosity Analysis

Earlier, the deviation of experimental viscosity data and ASHRAE Standard data of the base fluid has been analysed and presented in Fig. 16. The maximum standard deviation of about 0.27 found at the 80°C temperature of the base fluid. The viscosity of nanofluids (Al_2O_3 and CNC) with different volume concentrations (0.1%, 0.3%, and 0.5%) determined at four distinct temperatures such as 30°C, 50°C, 70°C and 80°C as shown in Fig. 15. In this study, viscosity increases with increasing volume fractions of nanoparticles but decreases when the temperature increased, and this phenomenon is similar to many previous studies [33, 34, 53]. The maximum viscosity obtained at 30°C of 0.5% volume concentration Al_2O_3 nanofluid whereas 0.3% volume concentration CNC nanofluid exhibited the highest viscosity. According to Newtonian Fluid theory, shear stress (τ) and shear rate ($\dot{\gamma}$) are straight and viscosity remains constant as defined Newtonian fluid [60]. In this study, the nanofluids (both Al_2O_3 and CNC) at various volume concentrations showed the non-Newtonian behaviour as shear viscosity increases with increasing shear stress at every individual temperature.

3.2.4 Specific Heat Analysis

The resulting data of specific heat capacity (C_p) of Al_2O_3 and CNC nanofluids (all volume concentrations) are shown in Fig. 17. Insufficient numerical and experimental studies had been conducted to determine the specific heat capacity of nanofluids at different temperature and volume concentrations. O'Hanley, Buongiorno [61] studied the specific heat capacity of nanofluids at various volume concentrations with different types of nanofluids (water-based alumina, silica, copper-oxide). The authors also used a size range (diameter) of nanoparticles. They revealed specific heat capacity decreased due to the crease of volume fractions of nanofluids. Sekhar and Sharma [62] found that the increasing volume concentration of nanofluids (water-based aluminium oxide) decline the specific heat capacity of nanofluids owing to the increase of thermal diffusivity of nanofluids. They also mentioned the increment of temperature causes the decrement of effective specific heat capacity of nanofluids. In this study, the adding of Al_2O_3 nanoparticles into the base fluid causes the loss of specific heat capacity and its increases (Fig. 17) with an increase in the mass fraction of nanoparticles into the base fluid [61], whereas 0.5% Al_2O_3 nanofluid showed the negative result at 30°C temperature. However, specific heat is an increasing trend due to the increasing temperature of Al_2O_3 nanofluid at all volume concentrations [63]. On the other hand, CNC nanofluids with all volume concentrations at a range of temperatures from 30°C to 80°C exhibited the negative

potentiality of specific heat capacity. Moreover, negativity increases with an increasing volume concentration of CNC nanofluids and with the improvement of temperature as well. In addition, CNC nanofluids at all volume concentrations showed fewer negativity results at 50°C temperature than at 30°C temperature. The smaller specific heat of solid particles compared to that of base fluid obviously will decrease the specific heat of the nanofluid mixture. The declining will be continued at the increment of the volumetric loading of particles [64]. Moreover, literature stated, there is good relation between specific heat and thermal conductivity, especially with thermal diffusivity as nanofluids can diffuse heat much better than base fluid such as Vajjha and Das [65] studied that among three of (Al_2O_3 , SiO_2 , CuO) CuO showed the highest thermal diffusivity at a defined temperature due to its lowest specific heat and high thermal conductivity values.

3.3 Efficiency Analysis of FPSC

The inlet and outlet temperature have been monitored several times for individual nanofluids and averaged the data, as shown in Table 7. Fig. 18 and Fig. 19 present the energy gain and efficiency scenario of FPSC. Fig. 18 presents the gradual enhancement of energy gain of 0.3% Al_2O_3 and 0.5% Al_2O_3 nanofluids at a temperature range of 30° to 80°C; while 0.3% CNC and 0.5% CNC nanofluids do not exhibit the linearity of energy gain increment at the same temperature. Both volume concentrations (0.3% and 0.5%) of CNC shows the decrement of energy gain at 50°C temperature. Moreover, the base fluid performs the discontinuation trend of energy gain in this system.

In addition, Fig. 19 illustrates the progressive enhancement of efficiency of Al_2O_3 nanofluids (both of 0.3% and 0.5% volume con.) whereas CNC nanofluids at both volume concentrations and base fluid do not maintain the gradual improvement of efficiency of solar collector. Besides, the maximum efficiency of 2.48% and 8.46% achieved by 0.5% Al_2O_3 and 0.5% CNC at 80°C temperature respectively; while there is a big difference between these two values of efficiency. On the other hand, the base fluid shows a maximum efficiency of 1.17% at 50°C temperature.

Currently, there are a few studies conducted with a mixture of water and ethylene glycol (60:40) as the base or working fluid for FPSC. This is due to the stability of nanoparticles in the water-EG mixture. Not all nanofluids stable in water/EG base fluid. It is different compared with water where nanoparticle easily stable specifically Al_2O_3 nanoparticles. A comparison

illustration of efficiency enhancement of FPSC using Al_2O_3 and CNC nanofluids with the experimental study of Meibodi, Kianifar [48] prepared as shown in Table 8. The authors investigated the thermal efficiency of FPSC using SiO_2 /water-EG nanofluids with 0%, 0.5%, 0.75% and 1% volume fraction of nanofluids at three mass flow rates including 0.018, 0.032 and 0.045 (kg/s). They concluded that the enhancement of the thermal efficiency of FPSC was 4 to 8% in maximum. Moreover, they remarked thermal efficiencies associated with concentrations of 0.75% and 1% are very close. The efficiency enhancement of FPSC using CNC/water-EG is higher than Al_2O_3 /water-EG and SiO_2 /water-EG nanofluids have been presented in Table 8. Even though the Al_2O_3 nanofluids exhibit lower efficiency enhancement, stability of Al_2O_3 nanofluids was good.

4. Conclusion

In this study, the energy gain and the efficiency of flat plate solar collector enhanced by using Al_2O_3 and CNC nanofluids (at 0.3% and 0.5% volume concentrations for both nanofluids) flowing through inside the tubes (header and riser) under direct solar radiation. Nanofluids play the role of working fluids. Therefore, findings of the works done throughout the study can be concluded as follows,

- 0.3% and 0.5% Al_2O_3 nanofluids performed good stability while 0.1% Al_2O_3 showed moderate stability. On the other hand, CNC nanofluids (all volume concentrations) exhibited the initial stage of instability.
- Maximum enhancement of thermal conductivity was 11.5% and 13.4% for CNC and Al_2O_3 nanofluids respectively at 80°C temperature.
- Dynamic viscosity of Al_2O_3 nanofluids (all volume con.) was decreasing and at 80°C temperature showed the lowest value of it, while CNC nanofluids (all volume fractions) show the decreasing trend of dynamic viscosity until at 70°C temperature. 0.5% Al_2O_3 nanofluid performed the lowest increment of the viscosity of about 4.9% at 80°C temperature whereas it was in maximal of 57% at 30°C temperature than the base fluid.
- Specific heat decreases with increasing nanofluids volume concentrations, but it is improved with the improvement of temperature. Moreover, CNC showed negative specific heat capacity which defines the mechanical instability that means the isothermal compressibility is negative or equivalent [66].
- Experimental data reveal that the outlet temperature enhanced by nanofluids and maximum increased by 0.5% Al_2O_3 nanofluid of about 4.4%.

- Energy gain and efficiency of flat plate solar collector improved too. Maximum efficiency of flat plate solar collector obtained of around 2.48% for 0.5% Al₂O₃ and 8.46% for 0.5% CNC nanofluids. Thus, about 5.8% efficiency can be improved using CNC/water-EG nanofluid in a flat plate solar collector.

Acknowledgment

The authors would like to acknowledge to University Malaysia Pahang (UMP), Ministry of Higher Education (MOHE) of Malaysia for the Research Grants RDU 190323 and Bangabandhu Science and Technology Fellowship Trust (Bangladesh) for the financial support and laboratory facilities provided by them throughout this study. Doctoral Fellowship Scheme conferred to Kaniz Farhana by the Ministry of Science and Technology (Bangladesh) is also greatly appreciated.

R. Saidur would like to acknowledge the financial support provided by the Sunway University through the project no. STR-RCTR-RCNMET-001-2019.

References

1. Viral, R. and D. Khatod, *Optimal planning of distributed generation systems in distribution system: A review*. Renewable and Sustainable Energy Reviews, 2012. **16**(7): p. 5146-5165.
2. Bell, S., et al., *Sociality and electricity in the United Kingdom: the influence of household dynamics on everyday consumption*. Energy research & social science, 2015. **9**: p. 98-106.
3. Gadisa, A., et al., *Transparent polymer cathode for organic photovoltaic devices*. Synthetic metals, 2006. **156**(16): p. 1102-1107.
4. Renewable Energy Policy Network, *The first decade : 2004 - 2014:10 years of renewable energy progress; Renewable energy policy Network For the 21st Century, France*. 2014.
5. Hussein, A.K., *Applications of nanotechnology to improve the performance of solar collectors-Recent advances and overview*. Renewable and Sustainable Energy Reviews, 2016. **62**: p. 767-792.
6. Alim, M., et al., *Analyses of entropy generation and pressure drop for a conventional flat plate solar collector using different types of metal oxide nanofluids*. Energy and Buildings, 2013. **66**: p. 289-296.
7. Struckmann, F., *Analysis of a flat-plate solar collector (Report no. 2008MVK160)*. Heat and Mass Transport., 2008.
8. Muhammad, M.J., et al., *Thermal performance enhancement of flat-plate and evacuated tube solar collectors using nanofluid: A review*. International Communications in Heat and Mass Transfer, 2016. **76**: p. 6-15.
9. Bashirnezhad, K., M. Ghavami, and A.A. Alrashed, *Experimental investigations of nanofluids convective heat transfer in different flow regimes: A review*. Journal of Molecular Liquids, 2017. **244**: p. 309-321.
10. Chol, S., *Enhancing thermal conductivity of fluids with nanoparticles*. ASME-Publications-Fed, 1995. **231**: p. 99-106.
11. Yu, W. and H. Xie, *A review on nanofluids: preparation, stability mechanisms, and applications*. Journal of Nanomaterials, 2012. **2012**: p. 1.
12. Feynman, R.P., *There's plenty of room at the bottom*. Resonance-Heidelberg, 2011. **16**(9): p. 890.
13. Hayat, T., et al., *Magnetohydrodynamic three-dimensional flow of viscoelastic nanofluid in the presence of nonlinear thermal radiation*. Journal of Magnetism and Magnetic Materials, 2015. **385**: p. 222-229.

14. Ganvir, R., P. Walke, and V. Kriplani, *Heat transfer characteristics in nanofluid—A review*. Renewable and Sustainable Energy Reviews, 2016.
15. Ghanbarpour, M., et al., *Improvement of heat transfer characteristics of cylindrical heat pipe by using SiC nanofluids*. Applied Thermal Engineering, 2015. **90**: p. 127-135.
16. Sara, O., et al., *Effect of suspended CuO nanoparticles on mass transfer to a rotating disc electrode*. Experimental Thermal and Fluid Science, 2011. **35**(3): p. 558-564.
17. Nagarajan, P., et al., *Nanofluids for solar collector applications: a review*. Energy Procedia, 2014. **61**: p. 2416-2434.
18. Panchal, K., *Nanofluid: A tool to increase the efficiency of solar collector*. International Journal for Innovative Engineering and Technology, 2015. **5**(2): p. 350-366.
19. Abitbol, T., et al., *Nanocellulose, a tiny fiber with huge applications*. Current opinion in biotechnology, 2016. **39**: p. 76-88.
20. Theivasanthi, T., et al., *Synthesis and characterization of cotton fiber-based nanocellulose*. International journal of biological macromolecules, 2017.
21. Yousefi, T., et al., *An experimental investigation on the effect of MWCNT-H₂O nanofluid on the efficiency of flat-plate solar collectors*. Experimental Thermal and Fluid Science, 2012. **39**: p. 207-212.
22. Moghadam, A.J., et al., *Effects of CuO/water nanofluid on the efficiency of a flat-plate solar collector*. Experimental Thermal and Fluid Science, 2014. **58**: p. 9-14.
23. Said, Z., et al., *Performance enhancement of a flat plate solar collector using titanium dioxide nanofluid and polyethylene glycol dispersant*. Journal of Cleaner Production, 2015. **92**: p. 343-353.
24. Verma, S.K., A.K. Tiwari, and D.S. Chauhan, *Performance augmentation in flat plate solar collector using MgO/water nanofluid*. Energy Conversion and Management, 2016. **124**: p. 607-617.
25. Verma, S.K., A.K. Tiwari, and D.S. Chauhan, *Experimental evaluation of flat plate solar collector using nanofluids*. Energy Conversion and Management, 2017. **134**: p. 103-115.
26. Ziyadanogullari, N.B., H. Yucel, and C. Yildiz, *Thermal performance enhancement of flat-plate solar collectors by means of three different nanofluids*. Thermal Science and Engineering Progress, 2018. **8**: p. 55-65.
27. Eltaweel, M. and A.A. Abdel-Rehim, *Energy and exergy analysis of a thermosiphon and forced-circulation flat-plate solar collector using MWCNT/Water nanofluid*. Case Studies in Thermal Engineering, 2019. **14**: p. 100416.
28. Gaos, Y.S., et al. *The performance of solar collector CPC (compound parabolic concentrator) type with three pipes covered by glass tubes*. in AIP Conference Proceedings. 2017. AIP Publishing.
29. Suresh, S., et al., *Synthesis of Al₂O₃-Cu/water hybrid nanofluids using two step method and its thermo physical properties*. Colloids and Surfaces A: Physicochemical and Engineering Aspects, 2011. **388**(1): p. 41-48.
30. Wei, B., et al., *Thermo-physical property evaluation of diathermic oil based hybrid nanofluids for heat transfer applications*. International Journal of Heat and Mass Transfer, 2017. **107**: p. 281-287.
31. Baghbanzadeh, M., et al., *Synthesis of spherical silica/multiwall carbon nanotubes hybrid nanostructures and investigation of thermal conductivity of related nanofluids*. Thermochimica acta, 2012. **549**: p. 87-94.
32. Nikkam, N., et al., *Fabrication, characterization and thermophysical property evaluation of SiC nanofluids for heat transfer applications*. Nano-Micro Letters, 2014. **6**(2): p. 178-189.
33. Ramachandran, K., et al., *Thermophysical properties measurement of nano cellulose in ethylene glycol/water*. Applied Thermal Engineering, 2017. **123**: p. 1158-1165.

34. Azmi, W., et al., *Heat transfer and friction factor of water and ethylene glycol mixture based TiO₂ and Al₂O₃ nanofluids under turbulent flow*. International Communications in Heat and Mass Transfer, 2016. **76**: p. 24-32.
35. Sundar, L.S., et al., *Nanodiamond-Fe₃O₄ nanofluids: preparation and measurement of viscosity, electrical and thermal conductivities*. International Communications in Heat and Mass Transfer, 2016. **73**: p. 62-74.
36. Abbasi, S.M., et al., *The effect of functionalisation method on the stability and the thermal conductivity of nanofluid hybrids of carbon nanotubes/gamma alumina*. Ceramics International, 2013. **39**(4): p. 3885-3891.
37. Agarwal, R., et al., *Synthesis, characterization, thermal conductivity and sensitivity of CuO nanofluids*. Applied Thermal Engineering, 2016. **102**: p. 1024-1036.
38. Kadirgama, K., et al., *Thermal analysis of SUS 304 stainless steel using ethylene glycol/nanocellulose-based nanofluid coolant*. The International Journal of Advanced Manufacturing Technology, 2018. **97**(5-8): p. 2061-2076.
39. Azmi, W., et al., *Heat transfer and friction factor of water based TiO₂ and SiO₂ nanofluids under turbulent flow in a tube*. International Communications in Heat and Mass Transfer, 2014. **59**: p. 30-38.
40. Esfe, M.H., et al., *Experimental determination of thermal conductivity and dynamic viscosity of Ag-MgO/water hybrid nanofluid*. International Communications in Heat and Mass Transfer, 2015. **66**: p. 189-195.
41. Samyalingam, L., et al., *Thermal analysis of cellulose nanocrystal-ethylene glycol nanofluid coolant*. International Journal of Heat and Mass Transfer, 2018. **127**: p. 173-181.
42. Chiam, H., et al., *Thermal conductivity and viscosity of Al₂O₃ nanofluids for different based ratio of water and ethylene glycol mixture*. Experimental Thermal and Fluid Science, 2017. **81**: p. 420-429.
43. Sun, Z., T. Deluca, and K. Mattison, *The size and rheology characterization of concentrated emulsions*. American laboratory, 2005. **37**(12): p. 8.
44. Kodre, K., et al., *Differential scanning calorimetry: A review*. Research and Reviews: Journal of Pharmaceutical Analysis, 2014. **3**(3): p. 11-22.
45. O'Neill, M., *Measurement of specific heat functions by differential scanning calorimetry*. Analytical chemistry, 1966. **38**(10): p. 1331-1336.
46. Demetzos, C., *Differential scanning calorimetry (DSC): a tool to study the thermal behavior of lipid bilayers and liposomal stability*. Journal of liposome research, 2008. **18**(3): p. 159-173.
47. Clas, S.-D., C.R. Dalton, and B.C. Hancock, *Differential scanning calorimetry: applications in drug development*. Pharmaceutical science & technology today, 1999. **2**(8): p. 311-320.
48. Meibodi, S.S., et al., *Experimental investigation on the thermal efficiency and performance characteristics of a flat plate solar collector using SiO₂/EG-water nanofluids*. International Communications in Heat and Mass Transfer, 2015. **65**: p. 71-75.
49. Gupta, M., V. Singh, and P. Katyal, *Synthesis and structural characterization of Al₂O₃ nanofluids*. Materials Today: Proceedings, 2018. **5**(14): p. 27989-27997.
50. Abdul Wahab, et al., *Solar energy systems – Potential of nanofluids*. Journal of Molecular Liquids 2019.
51. Awang, N., et al., *An experimental study on characterization and properties of nano lubricant containing Cellulose Nanocrystal (CNC)*. International Journal of Heat and Mass Transfer, 2019. **130**: p. 1163-1169.
52. Rance, G.A., et al., *van der Waals interactions between nanotubes and nanoparticles for controlled assembly of composite nanostructures*. ACS nano, 2010. **4**(8): p. 4920-4928.
53. Ramachandran, K., et al., *Investigation on effective thermal conductivity and relative viscosity of cellulose nanocrystal as a nanofluidic thermal transport through a combined experimental-Statistical approach by using Response Surface Methodology*. Applied Thermal Engineering, 2017. **122**: p. 473-483.

54. Ghadimi, A., R. Saidur, and H. Metselaar, *A review of nanofluid stability properties and characterization in stationary conditions*. International Journal of Heat and Mass Transfer, 2011. **54**(17): p. 4051-4068.
55. Korada, V.S. and N.H. Hamid, *Engineering Applications of Nanotechnology: From Energy to Drug Delivery*. 2017: Springer.
56. Sharma, S. and S.M. Gupta, *Preparation and evaluation of stable nanofluids for heat transfer application: a review*. Experimental Thermal and Fluid Science, 2016. **79**: p. 202-212.
57. Wei, B., C. Zou, and X. Li, *Experimental investigation on stability and thermal conductivity of diathermic oil based TiO₂ nanofluids*. International Journal of Heat and Mass Transfer, 2017. **104**: p. 537-543.
58. Wen, D. and Y. Ding, *Experimental investigation into convective heat transfer of nanofluids at the entrance region under laminar flow conditions*. International journal of heat and mass transfer, 2004. **47**(24): p. 5181-5188.
59. Ding, Y. and D. Wen, *Particle migration in a flow of nanoparticle suspensions*. Powder Technology, 2005. **149**(2-3): p. 84-92.
60. Bagnold, R.A., *Experiments on a gravity-free dispersion of large solid spheres in a Newtonian fluid under shear*. Proceedings of the Royal Society of London. Series A. Mathematical and Physical Sciences, 1954. **225**(1160): p. 49-63.
61. O'Hanley, H., et al., *Measurement and model validation of nanofluid specific heat capacity with differential scanning calorimetry*. Advances in Mechanical Engineering, 2012. **4**: p. 181079.
62. Sekhar, Y.R. and K. Sharma, *Study of viscosity and specific heat capacity characteristics of water-based Al₂O₃ nanofluids at low particle concentrations*. Journal of experimental Nanoscience, 2015. **10**(2): p. 86-102.
63. Singh, R.K., et al., *Experimental investigation of thermal conductivity and specific heat of nanoparticles mixed cutting fluids*. Materials Today: Proceedings, 2017. **4**(8): p. 8587-8596.
64. Murshed, S.S., *Simultaneous measurement of thermal conductivity, thermal diffusivity, and specific heat of nanofluids*. Heat Transfer Engineering, 2012. **33**(8): p. 722-731.
65. Vajjha, R.S. and D.K. Das, *A review and analysis on influence of temperature and concentration of nanofluids on thermophysical properties, heat transfer and pumping power*. International Journal of Heat and Mass Transfer, 2012. **55**(15-16): p. 4063-4078.
66. Das, C., S.D. Gupta, and A. Mekjian, *Negative specific heat in a thermodynamic model of multifragmentation*. Physical Review C, 2003. **68**(1): p. 014607.

List of Figures

- Fig. 1. Preparation process of nanofluids.
- Fig. 2. Specific heat measurement equipment (a) DSC Linseis 1000 (b) electric balance, and (c) aluminium crucible.
- Fig. 3. The experimental setup.
- Fig. 4. Process flow of the experimental work.
- Fig. 5. FESEM morphology of Al_2O_3 nanoparticles (Magnification x70,000; WD 9.9 mm).
- Fig. 6. EDX spectrum of Al_2O_3 nanoparticles.
- Fig. 7. TEM morphology of Al_2O_3 nanofluids (Magnification x100,000).
- Fig. 8. FESEM micrograph of CNC nanoparticles (a) film form (Magnification x70,000; WD 9.3 mm) and (b) powder form (Magnification x70,000; WD 9.4 mm).
- Fig. 9. EDX micrograph of CNC nanoparticles.
- Fig. 10. TEM image of CNC nanoparticles (Magnification x62,000).
- Fig. 11. TEM morphology of CNC nanofluids (Magnification x50,000).
- Fig. 12. Quantitative analysis of the stability of nanofluids.
- Fig. 13. Thermal conductivity of Al_2O_3 and CNC nanofluids at various temperatures.
- Fig. 14. Graphical presentation of error difference of thermal conductivity of experimental and ASHRAE Standard data of base fluid.
- Fig. 15. Temperature dependence of viscosity of Al_2O_3 and CNC nanofluids.
- Fig. 16. Variation of error of dynamic viscosity of experimental and ASHRAE Standard data of base fluid.
- Fig. 17. Evaluation of specific heat of Al_2O_3 and CNC nanofluids correlated with temperature.
- Fig. 18. Energy gain of flat plate solar collector.
- Fig. 19. Improvement of efficiency of flat plate solar collector.

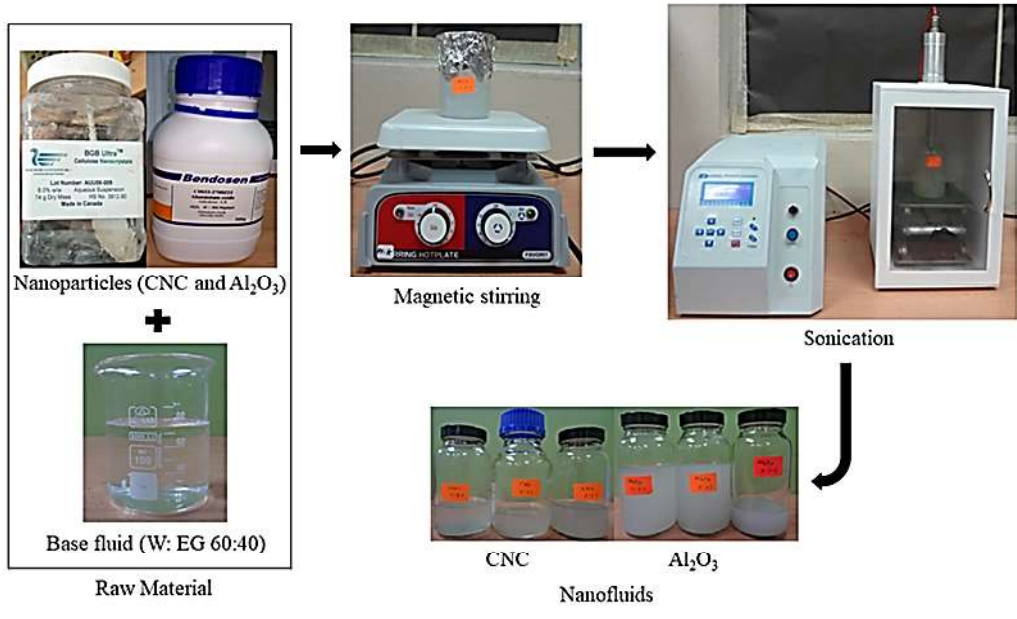


Fig. 1. Preparation process of nanofluids.



(a)



(b)



(c)

Fig. 2. Specific heat measurement equipment (a) DSC Linseis 1000 (b) electric balance, and (c) aluminium crucible.

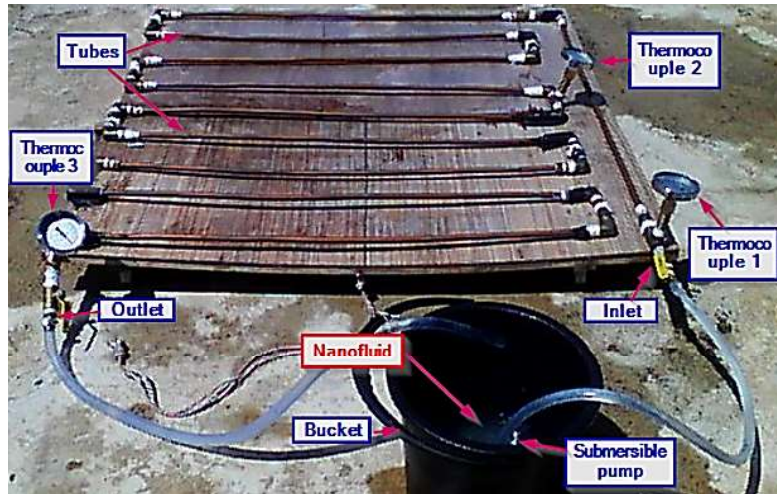


Fig. 3. The experimental setup.

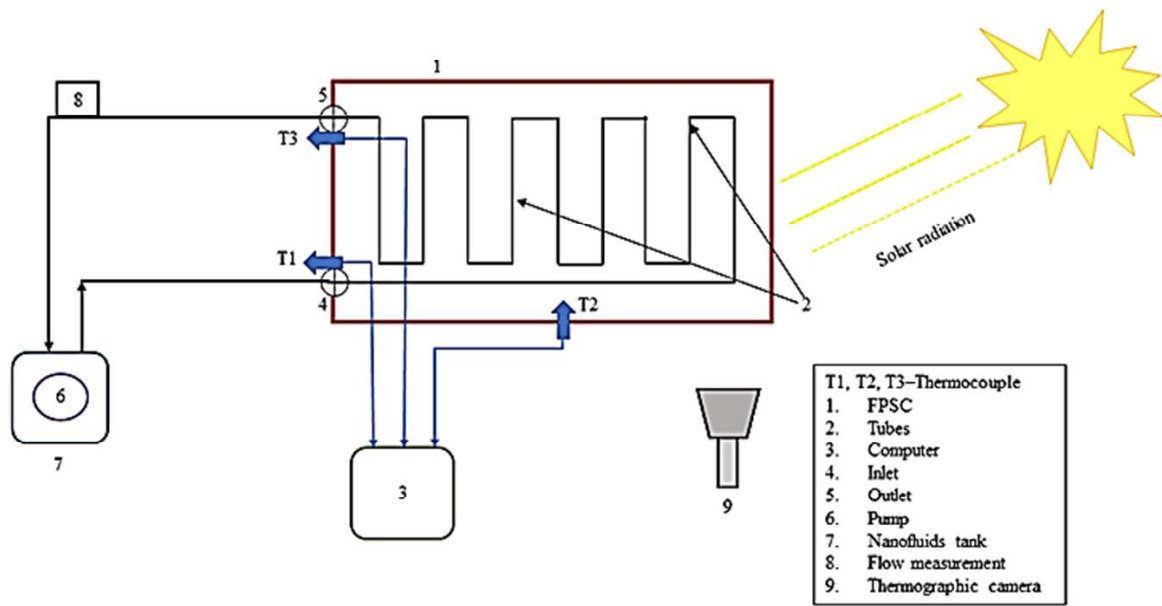


Fig. 4. Process flow of the experimental work.

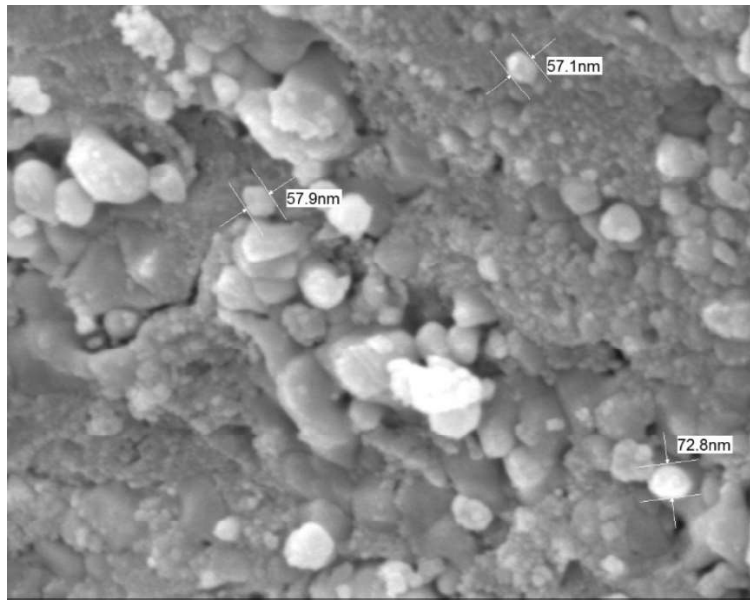


Fig. 5. FESEM morphology of Al₂O₃ nanoparticles (Magnification x70,000; WD 9.9 mm).

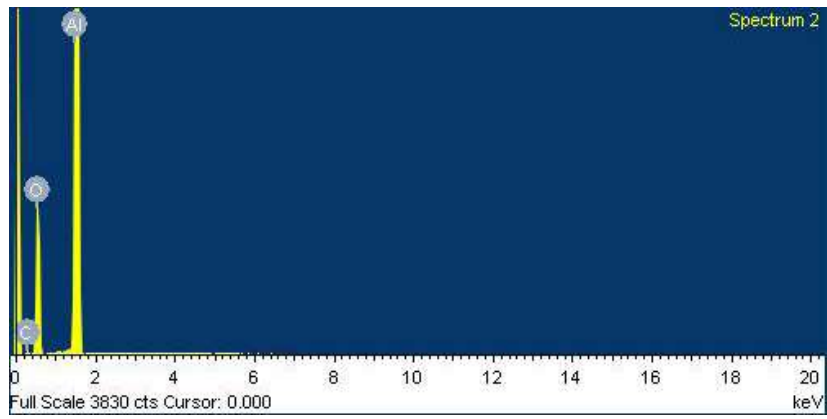


Fig. 6. EDX spectrum of Al₂O₃ nanoparticles.

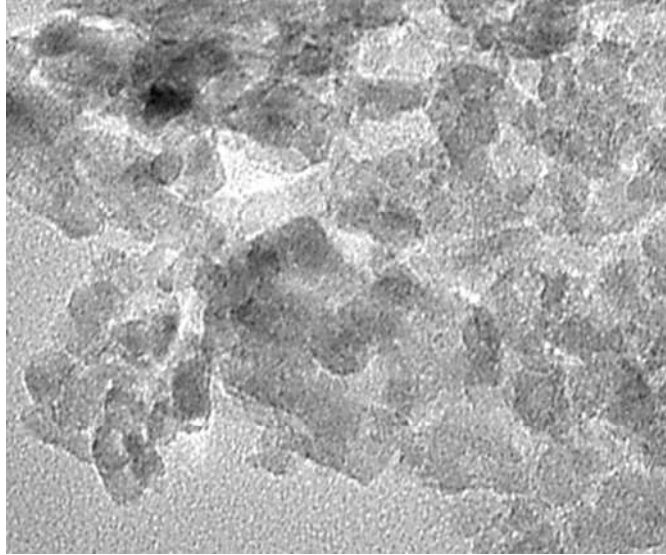


Fig. 7. TEM morphology of Al₂O₃ nanofluids (Magnification x100,000).

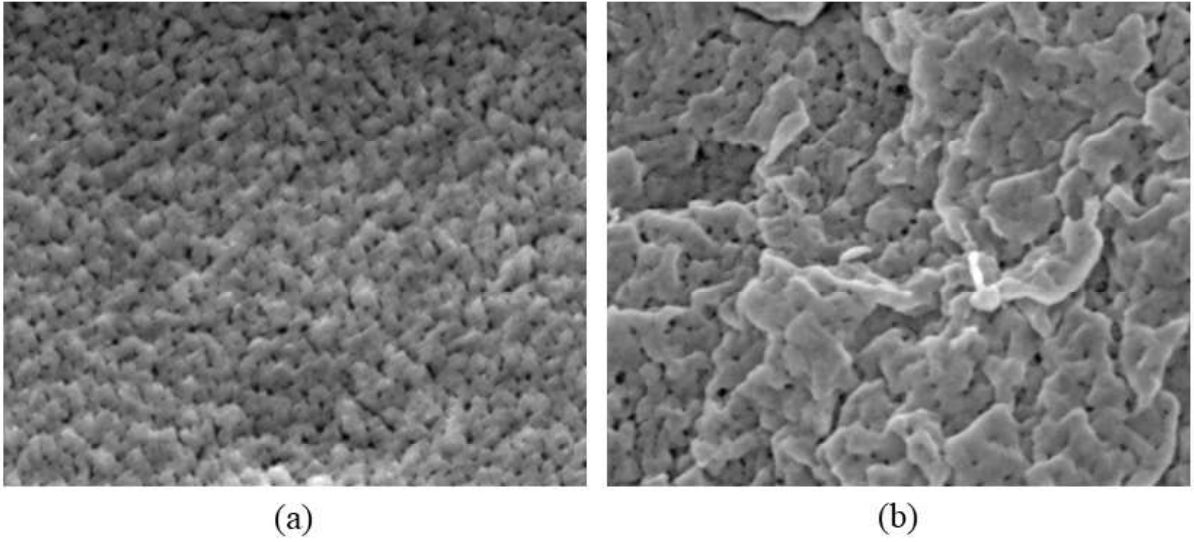


Fig. 8. FESEM micrograph of CNC nanoparticles (a) film form (Magnification x70,000; WD 9.3 mm) and (b) powder form (Magnification x70,000; WD 9.4 mm).

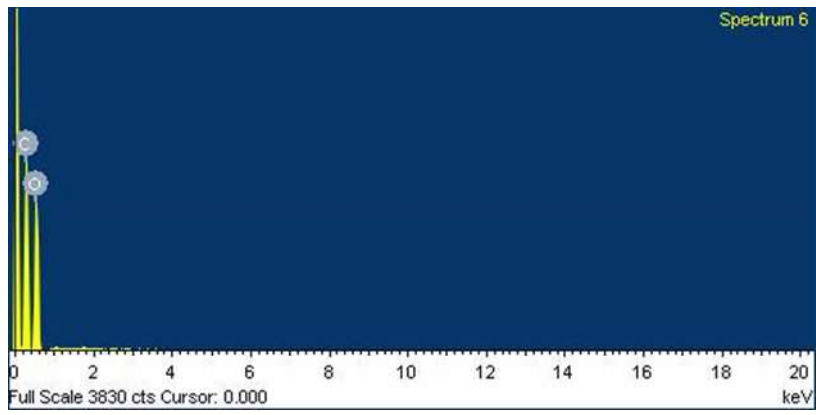


Fig. 9. EDX micrograph of CNC nanoparticles.

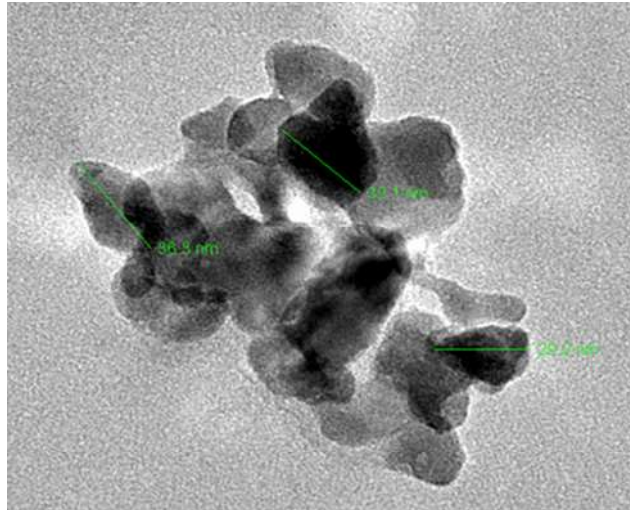


Fig. 10. TEM image of CNC nanoparticles (Magnification x62,000).

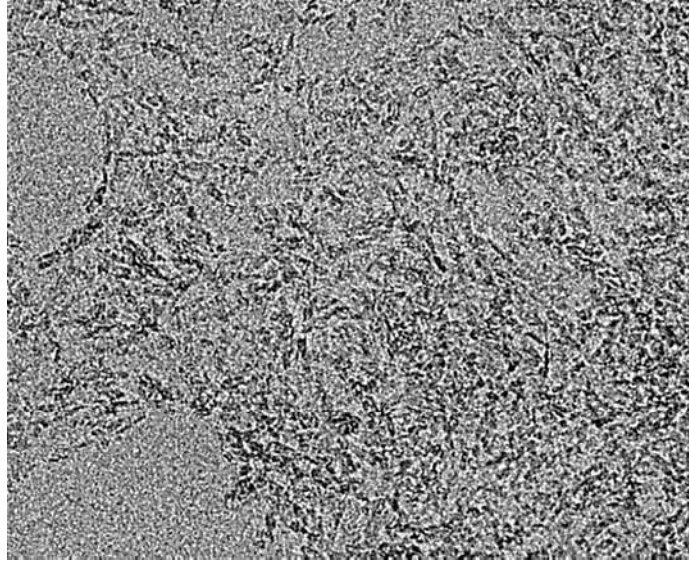


Fig. 11. TEM morphology of CNC nanofluids (Magnification x50,000).

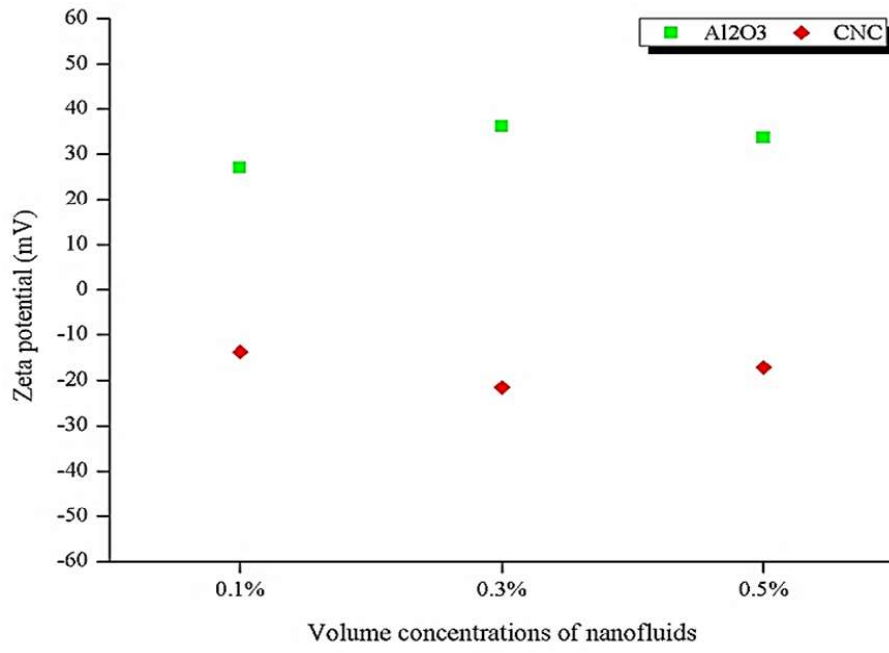


Fig. 12. Quantitative analysis of the stability of nanofluids.

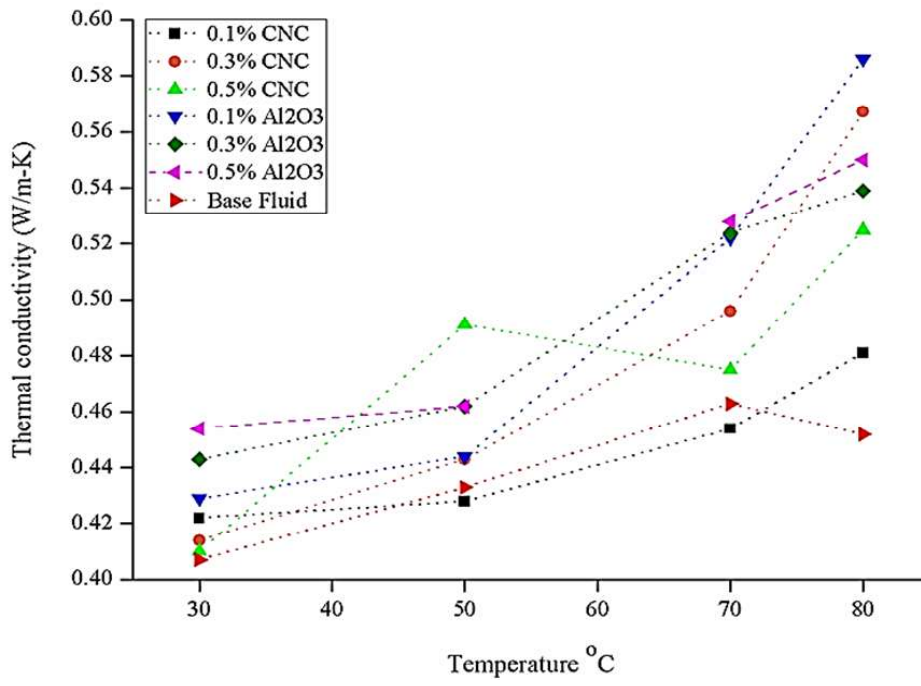


Fig. 13. Thermal conductivity of Al₂O₃ and CNC nanofluids at various temperatures.

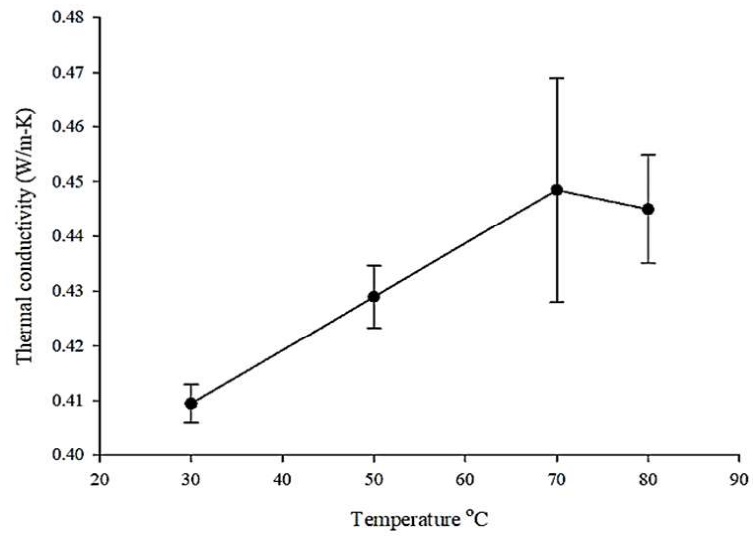


Fig. 14. Graphical presentation of error difference of thermal conductivity of experimental and ASHRAE Standard data of base fluid.

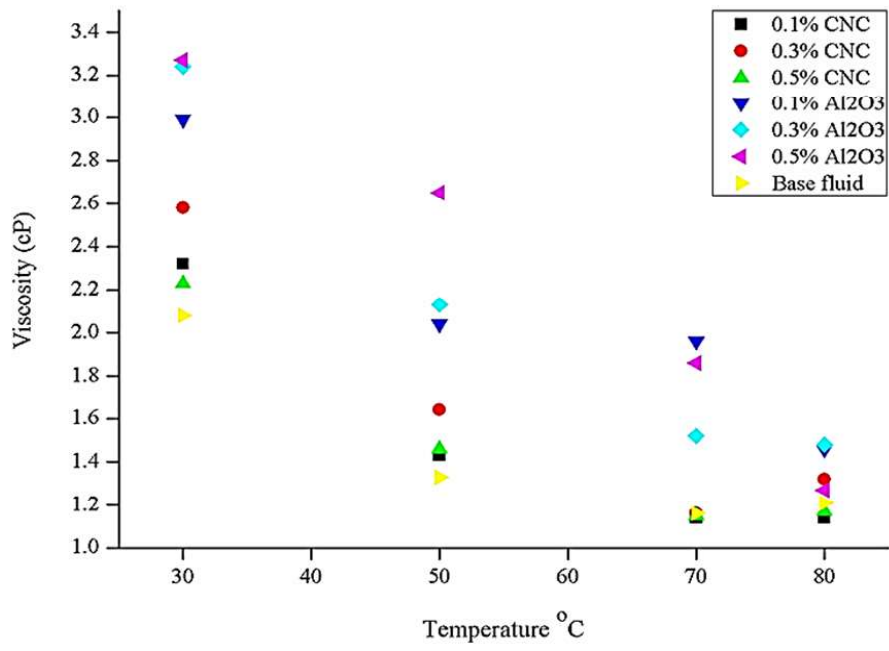


Fig. 15. Temperature dependence of viscosity of Al₂O₃ and CNC nanofluids.

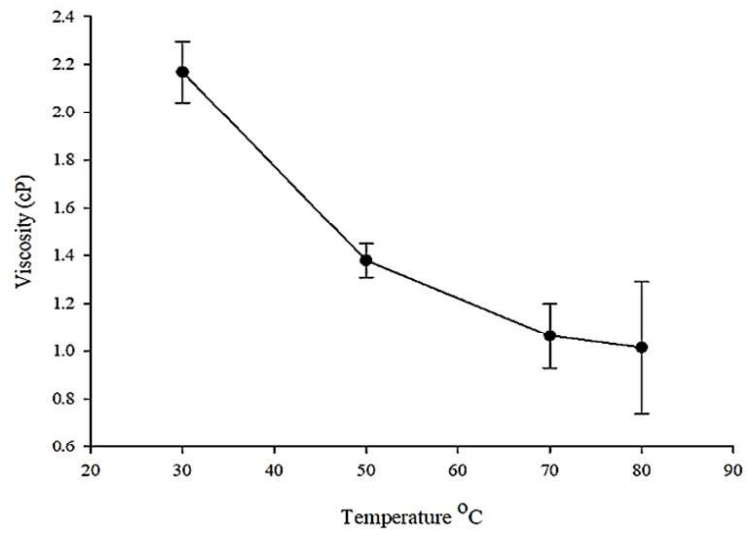


Fig. 16. Variation of error of dynamic viscosity of experimental and ASHRAE Standard data of base fluid.

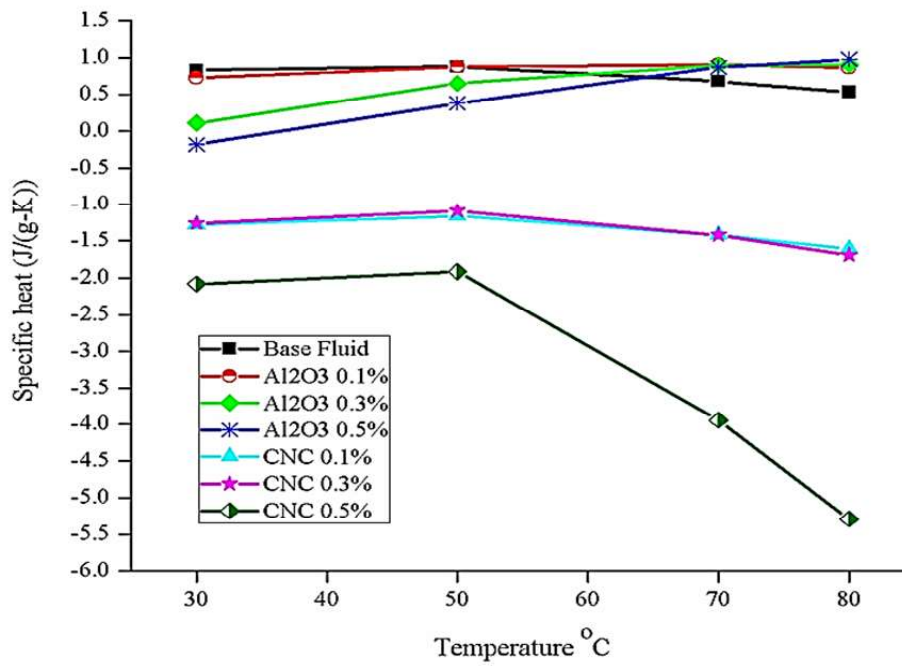


Fig. 17. Evaluation of specific heat of Al₂O₃ and CNC nanofluids correlated with temperature.

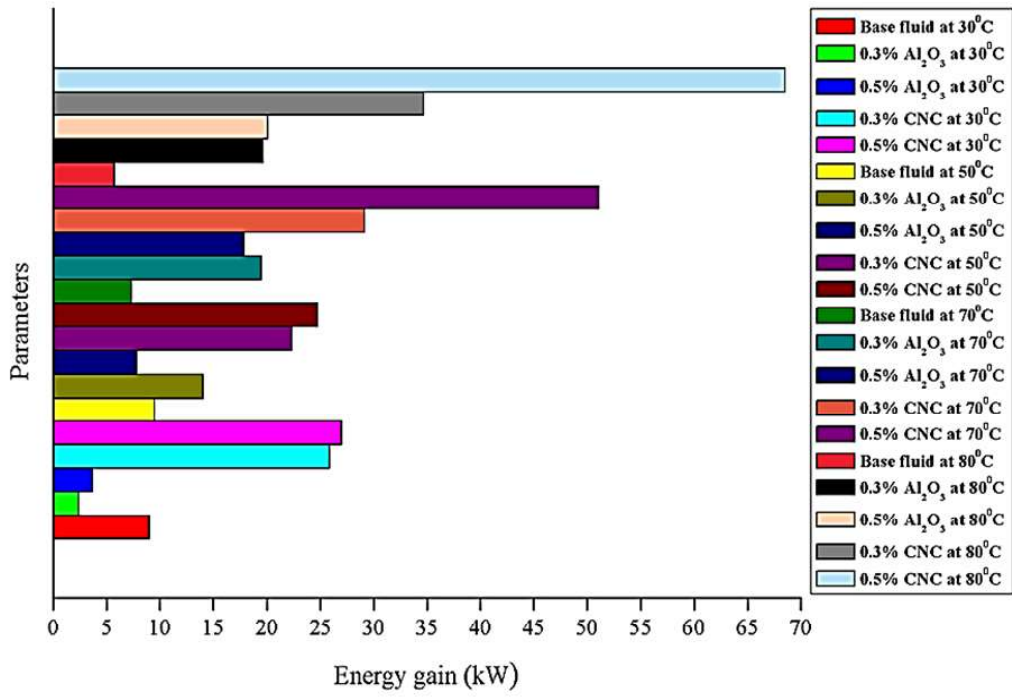


Fig. 18. Energy gain of flat plate solar collector.

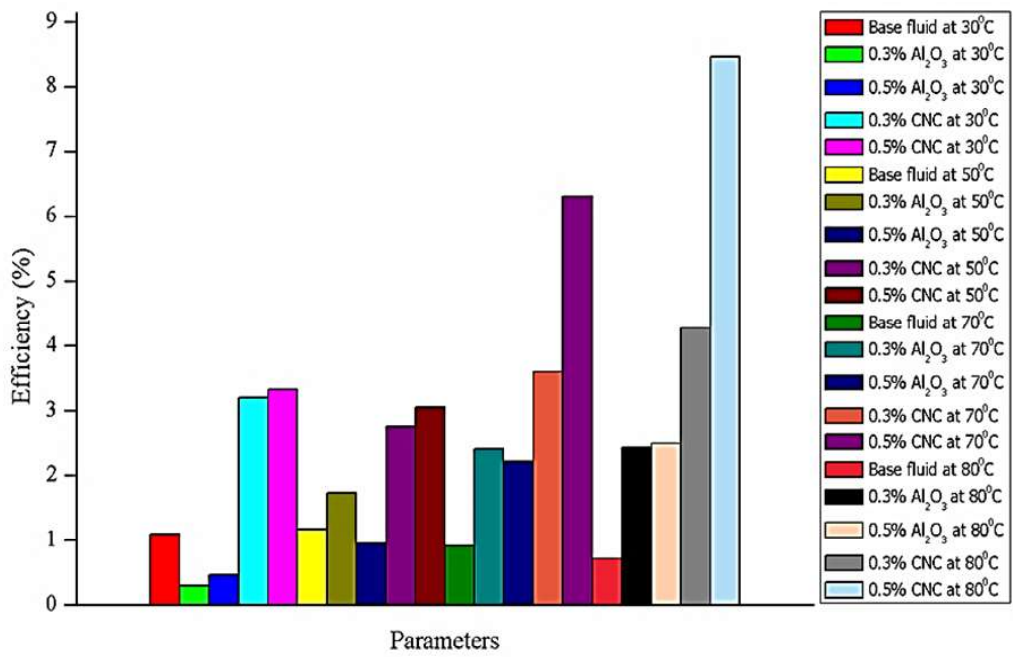


Fig. 19. Improvement of efficiency of flat plate solar collector.

List of Tables

Table 1 Specification parameters of CNC [28].

Table 2 Specification of the tubes of FPSC.

Table 3 List of apparatus of the experimental setup of FPSC.

Table 4 Quantification results of Al₂O₃ nanoparticles.

Table 5 Quantification results of CNC nanoparticles.

Table 6 Evaluation of qualitative stability measurement of nanofluids.

Table 7 Experimental data of temperature (°C) of nanofluids.

Table 8 Comparison of efficiency of FPSC with other research study.

Table 1

Specification parameters of CNC [28].

Parameter	Value
Crystallinity index	80%
Crystal length	100-150 nm
Crystal diameter	9-14 nm
Hydrodynamic Diameter	150nm

Table 2

Specification of the tubes of FPSC.

Properties	Parameters
Inner diameter	12.5
Outer diameter (mm)	12.7
Number of tubes	10
Total length (m) of the tubes	12.325
Tube material	Copper

Table 3

List of apparatus of the experimental setup of FPSC.

Sr. no	Name of the apparatus	Characteristics	Number of apparatus
1	Frame	Wooden	One
2	Tubes	Copper; outer diameter 12.7 mm; inner diameter 12.5 mm; length 1m	Ten
3	Thermocouples	Sensing element: coiled bimetallic	Three
4	Pump (Dolphin PA500)	Electrical submersible filter	One
5	Bucket	Plastic	One

Table 4Quantification results of Al₂O₃ nanoparticles.

Element	Weight %	Standard deviation	Atomic %	Standard deviation
Oxygen, O	49.49	5.34	59.73	3.36
Aluminium, Al	45.90	9.41	32.85	8.35

Table 5

Quantification results of CNC nanoparticles.

Element	Weight %	Standard deviation	Atomic %	Standard deviation
Carbon, C	47.22	1.19	54.37	1.18
Oxygen, O	52.78	1.19	45.63	1.18

Table 6

Evaluation of qualitative stability measurement of nanofluids.

Nanofluid	After preparation	After seven days
Al ₂ O ₃		
CNC		

Table 7

Experimental data of temperature (°C) of nanofluids.

Parameters	Outlet temperature (°C)	Inlet temperature (°C)
Base fluid	42.66	41.66
0.3% Al ₂ O ₃	42.4	40.4
0.5% Al ₂ O ₃	45.1	43.2
0.3% CNC	44.88	42.9
0.5% CNC	43.6	42.4

Table 8

Comparison of efficiency of FPSC with other research study.

Nanofluids	Efficiency (%)	
	Experimental results	Meibodi, Kianifar [49]
CNC/water-EG	8.46	-
SiO ₂ /water-EG	-	8
Al ₂ O ₃ /water-EG	2.48	-

Declaration of interests

The authors declare that they have no known competing financial interests or personal relationships that could have appeared to influence the work reported in this paper.

The authors declare the following financial interests/personal relationships which may be considered as potential competing interests: